Available online at www.sciencedirect.com
SCIENCE DIRECT
Journal of Photochemistry and Photobiology A: Chemistry 174 (2005) 28–37
Journal of Photochemistry and Photobiology A:Chemistry
www.elsevier.com/locate/jphotochem

Crystal structures and luminescence properties of $[Eu(ODA)\cdot(phen)\cdot 4H_2O]^+$, $[Tb(ODA)\cdot(phen)\cdot 4H_2O]^+$ and $[Tb(ODA)_3]^{3-}$ (ODA: oxydiacetate, phen: 1,10-phenanthroline)

Jun-Gill Kang *, Tack-Jin Kim, Hee-Jung Kang, Sung Kwon Kang

Department of Chemistry, Chungnam National University, Daejeon 305-764, Republic of Korea

Received 18 November 2004; received in revised form 17 January 2005; accepted 24 January 2005
Available online 19 March 2005

Abstract

Two novel complexes of Eu(III) and Tb(III) with mixed oxydiacetate (ODA) and 1,10-phenanthroline (phen) ligands and a Tb(III) complex with homoleptic ODA were prepared and their crystal structures were determined: $[Eu(ODA)\cdot(phen)\cdot 4H_2O]Cl\cdot 5H_2O$, monoclinic, $P2_1/n$, $a = 12.3197(12)$ Å, $b = 16.7992(17)$ Å, $c = 12.6754(10)$ Å, $\beta = 107.981(8)^\circ$, $V = 2495.2(4)$ Å^3, $Z = 4$, $R(|F|) = 0.0324$ for 5728 data; $[Tb(ODA)\cdot(phen)\cdot 4H_2O]Cl\cdot 5H_2O$ monoclinic, $P2_1/n$, $a = 12.2846(13)$ Å, $b = 16.7560(14)$ Å, $c = 12.6681(11)$ Å, $\beta = 108.144(8)^\circ$, $V = 2478.0(4)$ Å^3, $Z = 4$, $R(|F|) = 0.0279$ for 4364 data; $Na_3[Tb(ODA)_3]\cdot 8H_2O$ monoclinic, Cc, $a = 15.751(3)$ Å, $b = 9.8030(14)$ Å, $c = 18.189(4)$ Å, $\beta = 105.513(15)^\circ$, $V = 2706.2(9)$ Å^3, $Z = 4$, $R(|F|) = 0.0406$ for 3435 data. In these structures, the rare earth ions satisfy nine-coordination via binding to tridentate ODA, bidentate phen or water molecules. The geometry of the nine-coordinate polyhedron is discussed in terms of the dihedral angle and the mean plane.

Photoluminescence (PL) and excitation spectra of Eu(III) and Tb(III) complexes with mixed ODA and phen ligands and with homoleptic ODA are reported. The complexes of $[Eu(ODA)\cdot(phen)\cdot 4H_2O]^+$ and $[Tb(ODA)\cdot(phen)\cdot 4H_2O]^+$ excited by UV light produce very bright red and green emissions, respectively, via the nonradiative energy-transfer from phen to the metals. For $[Eu(ODA)\cdot(phen)\cdot 4H_2O]^+$ and $[Tb(ODA)\cdot(phen)\cdot 4H_2O]^+$, the quantum yields of the sensitized luminescence ($Q = 6.6$ and $Q = 75.7\%$, respectively) are much greater than those of the nonsensitized luminescence ($Q = 2.0$ and $Q = 21.0\%$, respectively).

Keywords: Europium; Terbium; Oxydiacetate; 1,10-Phenanthroline; Crystal structure; Photoluminescence and excitation; Energy-transfer; Quantum yield

1. Introduction

The Eu^{3+} and Tb^{3+} complexes have attracted great attentions due to their unique luminescence properties, including hypersensitivity to the coordination environment, narrow bandwidth and millisecond lifetime [1,2]. The absorption coefficients of these ions, however, are very small. In an effort to obtain high-efficient luminescence, an organic ligand is introduced as a sensitizer to complexes of these metals. Most of the excitation energy is transferred from the sensitizing ligand to the rare earth ions and this results in the enhanced red or blue luminescence. Typical ligands include the combination of β-diketons and a sensitizer, such as 1,10-phenanthroline (phen), bipyridine, or terpyridine [3]. The design and investigation of Eu^{3+} and Tb^{3+} complexes with these organic ligands has attracted great interest due to their applications in efficient light-conversion molecular devices (LCMDs) and organic light-emitting diodes (OLEDs) [4]. Rare earth complexes with polycarboxylates, however, have a good potential for light emitting devices due to their preferable ionic bonds and hypersensitive luminescence under reduced site-symmetry. Oxydiacetate (ODA) has the simplest polycarboxylate structure, but is a versatile complexing agent with five potential oxygen-donor atoms. Previously, we reported X-ray structure and optical property of Er(III) complex with mixed ODA and phen ligands [5]. In this study, we extended our works to Eu(III) and Tb(III) complexes. We pre-

* Corresponding author. Tel.: +82 42 821 6548; fax: +82 42 823 1360.
E-mail address: jgkang@cnu.ac.kr (J.-G. Kang).

1010-6030/$ – see front matter © 2005 Elsevier B.V. All rights reserved.
doi:10.1016/j.jphotochem.2005.01.019

pared Eu(III) and Tb(III) complexes using ODA as a bridging chelate and phen as a sensitizer, and characterized their crystal structures and luminescence properties. Crystallographic studies of ODA complexes have been reported for trivalent lanthanide ions (Ce, Nd, Eu, Gd, Yb, and mixed Y and La), in which ODA formed complexes as tridentate ligand [6–9]. However, the crystal structure and the luminescence property of Tb(III) complex with ODA have not been reported. This paper also reports the structural and optical properties of a Tb(III) complex with homoleptic ODA ligand.

2. Experimental

2.1. Crystal growth and composition analysis

$[Eu(ODA)\cdot(phen)\cdot 4H_2O]Cl\cdot 5H_2O$: $EuCl_3\cdot 6H_2O$ (99.9%), oxydiacetic acid ($ODAH_2$, 98%) and 1.10-phenanthroline (phen, >99%) were purchased from Aldrich and used without further purification. ODAH2 (0.268 g, 2 mmol) was added to a solution of europium chloride hexahydrate (0.366 g, 1 mmol) and phen (0.180 g, 1 mmol) in water (10 mL). The pH of the solution was adjusted to between 5 and 6 with dilute NaOH and the resultant solution was stirred for 2 h at room temperature. The resultant solution was colorless initially, but changed to pink and finally to orange. Colorless prismatic crystals of the complex were obtained by the slow evaporation method.

The cations were analyzed quantitatively with a Perkin-Elmer 2380 atomic absorption spectrometer. The analyses of carbon, hydrogen, nitrogen and oxygen contents were made on a CE EA-1110 elemental analyzer. An ion chromatographic analysis was also conducted to determine the amount of chloride ion in the crystals. Anal. Found: Eu 22.6; C 29.1; H 4.5; N 3.3; O 30.1; Cl 5.2%. Cal. For $Eu(ODA)\cdot(phen)Cl\cdot 9H_2O$: Eu 23.0; C 29.0; H 4.5; N 4.2; O 34.0; Cl 5.4%.

$[Tb(ODA)\cdot(phen)\cdot 4H_2O]Cl\cdot 5H_2O$: $TbCl_3\cdot 6H_2O$ (99.9%) was purchased from Aldrich and used without further purification. ODAH2 (0.268 g, 2 mmol) was added to a solution of terbium chloride hexahydrate (0.374 g, 1 mmol) and phen (0.180 g, 1 mmol) in water (5 mL). Crystals of $[Tb(ODA)\cdot(phen)\cdot 4H_2O]Cl\cdot 5H_2O$ were grown by slow evaporation of the resultant solution at a pH of 5–6, at room temperature. Colorless prismatic crystals of the complex were obtained from the orange colored solution. Anal. Found: Tb 23.8; C 29.2; H 4.5; N 4.3; Cl 5.0%. Cal. For $Tb(ODA)\cdot(phen)Cl\cdot 9H_2O$: Tb 23.8; C 28.7; H 4.5; N 4.2; Cl 5.3%.

$Na_3[Tb(ODA)_3]\cdot 8H_2O$: Terbium chloride hexahydrate (0.358 g, 1 mmol) and ODAH2 (0.402 g, 3 mmol) were dissolved in 5 mL water. The pH of the mother solution was adjusted at 5–6 with a mild NaOH solution. Colorless prismatic crystals of the complex were obtained from the colorless solution by the slow evaporation method. Anal. Found: Na 9.47; Tb 20.84; C 18.38; H 2.67; O 46.97%. Cal. For $Na_3[Tb(ODA)_3]\cdot 8H_2O$: Na 8.98; Tb 20.69; C 18.76; H 3.67; O 47.90%.

2.2. TG/DTG analysis

The TG and DTG spectra of the prepared complexes were recorded up to 500 °C using a Setaram TGA-92 to find the number of water molecules in the complexes. Two distinctive steps due to weight loss were found in the temperature ranges of 50–120 °C and 270–400 °C for $[Eu(ODA)\cdot(phen)\cdot 4H_2O]Cl\cdot 5H_2O$. A 24% weight loss occurred in the first step; this corresponds to the wt.% of the water molecules included in the complexes, which have a theoretical value of 24.2 wt.%. The weight loss during the second step was 27.6%, which almost equals to the theoretical 27.0 wt.% of phen in the complex. The TG and DTG spectra of $[Tb(ODA)\cdot(phen)\cdot 4H_2O]Cl\cdot 5H_2O$ are very similar to those of $[Eu(ODA)\cdot(phen)\cdot 4H_2O]Cl\cdot 5H_2O$.

2.3. Determination and refinement of the X-ray structure

Intensity data were collected at room temperature on a Bruker P4 diffractometer using graphite monochromated Mo Kα radiation. The intensities were corrected for Lorentz-polarization effects, and empirical absorption correction (Ψ scan) was also applied. The structures of the titled compounds were solved by applying the direct method using a Bruker SHELXTL [10] and refined by a full-matrix least-squares refinement on F using SHELEX97 [11]. The non-H atoms were refined with anisotropic displacement parameters. The crystal data and refinement results are summarized in Table 1.

2.4. Spectroscopic measurements

The luminescence and excitation spectra were measured at 90° angle with an ARC 0.5 m Czerny–Turner monochromator equipped with a cooled Hamamatsu R-933-14 PM tube. The sample was irradiated with a He–Cd 325-nm laser line or the light from an Oriel 1000 W Xe lamp (working power, 400 W) passing through an Oriel MS257 monochromator. To measure low-temperature luminescence and excitation spectra, the samples were placed on the cold finger of a closed-cycle helium refrigerator (CTI-cryogenics). To determine the decay time, we used a time-correlated single photon counting system with an Edinburg FL 900 spectrophotometer.

The luminescence quantum yield, defined by

$$Q = \frac{\text{number of photons emitted}}{\text{number of photons absorbed}} \quad (1)$$

was determined based on the method described previously [12,13]. The recorded spectra for the quantum yield were corrected for the spectral response of the system using an Oriel 45-W quartz tungsten halogen lamp standard. All measurements were repeated three times. No significant experimental error was found.

Table 1
Crystal data and structure refinement for [Eu(ODA)·(phen)·4H_2O]Cl·5H_2O, [Tb(ODA)·(phen)·4H_2O]Cl·5H_2O and Na_3[Tb(ODA)$_3$]·8H_2O

Formula	$C_{16}H_{28}O_{14}N_2EuCl$	$C_{16}H_{30}O_{14}N_2TbCl$	$C_{12}H_{28}O_{23}Na_3Tb$
fw	659.81	668.79	768.23
Crystal system	Monoclinic	Monoclinic	Monoclinic
Space group	$P2_1/n$	$P2_1/n$	Cc
a (Å)	12.3197(12)	12.2846(13)	15.751(3)
b (Å)	16.7992(17)	16.7560(14)	9.8030(14)
c (Å)	12.6754(10)	12.6681(11)	18.189(4)
β (°)	107.981(8)	108.144(8)	105.513(15)
V (Å^3)	2495.2(4)	2478.0(4)	2706.2(9)
Z	4	4	4
d_{cal} (mg m^{-3})	1.756	1.793	1.866
F(0 0 0)	1320	1336	1528
μ (mm^{-1})	2.689	3.031	2.757
θ range (°)	4.89–12.55	2.02–25.00	2.32–27.50
h k l range	−1 to 16, −1 to 21, −16 to 15	−1 to 14, −1 to 19, −15 to 14	−20 to 1, −1 to 12, −22 to 23
Reflections collected/unique [*R*(int)]	6957/5728 [0.0414]	5393/4364 [0.0351]	3842/3435 [0.0421]
Completeness (%) [to θ/°]	100 [27.49]	100 [25.00]	99.9 [27.50]
Data, restraints, parameters	5728, 0, 340	4364, 0, 380	3435, 2, 328
Goodness-of-fit on F^2	1.058	1.040	1.056
R1, *w*R2[$I > 2\sigma(I)$]			
All data	0.0324, 0.0756	0.0279, 0.0682	0.0406, 0.1047
	0.0477, 0.0880	0.0339, 0.0741	0.0409, 0.1054
Extinction coefficient	0.00111(17)	0.0035(2)	0.0113(5)
Largest diff. peak, hole (e Å^{-3})	1.297, −0.708	1.135, −1.062	2.655, −1.450

The function minimized was $\left[\sum w(|F_0| - |F_c|)^2 / \sum wF_0^2\right]^{1/2}$, (a) $w = 1/[\sigma^2(F_0^2) + (0.0390P)^2 + 2.5289P]$, (b) $w = 1/[\sigma^2(F_0^2) + (0.145P)^2 + 45.3766P]$, (c) $w = 1/[\sigma^2(F_0^2) + (0.0866P)^2 + 4.6697P]$, where $P = (F_0^2 + 2F_c^2)/3$.

3. Results and discussion

3.1. Description of structure

[Eu(ODA)·(phen)·4H_2O]$^+$: The complex crystallizes in the monoclinic space $P2_1/n$. Fig. 1(a) shows a perspective view of the crystalline forms for the [Eu(ODA)·(phen)·4H_2O]$^+$ complex. Selected bond lengths and angles are given in Table 2. In the complex, the Eu(III) ions satisfy nine-coordination via binding to tridentate ODA, bidentate phen, and four water molecules. The Eu–O distances are 2.346(3) and 2.368(3) Å for the two Eu–carboxylate oxygen bonds, and 2.530(3) Å for the Eu–ether oxygen bond. These values are slightly longer than the respective Er–O distances (2.289(3) and 2.312(3) Å for the Er–carboxylate oxygen bonds, and 2.493(3) Å for the Er–ether oxygen bond) [5]. The Eu–N distances are 2.597(4) and 2.609(4) Å. These values are also longer than the respective Er–N distances (2.538(6) and

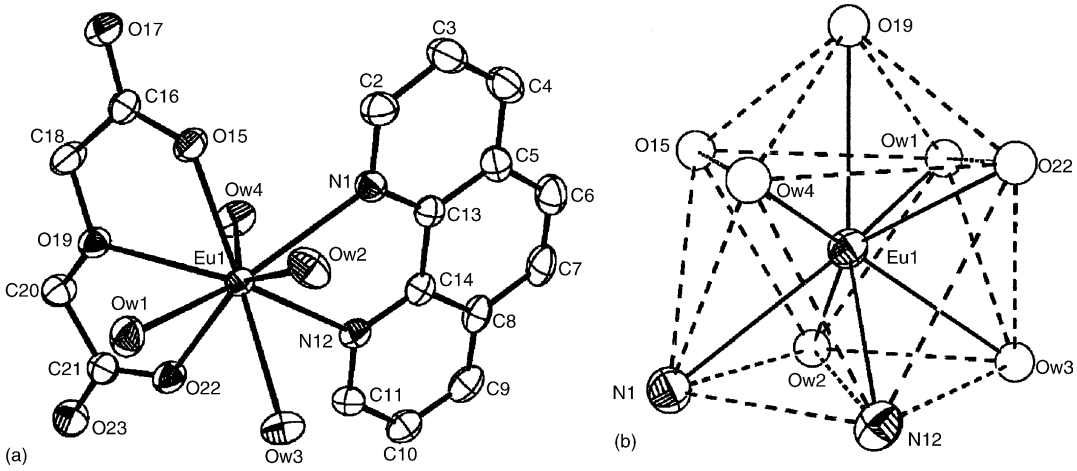

Fig. 1. View of the [Eu(ODA)·(phen)·4H_2O]$^+$ cation showing atom labeling and ellipsoids at 50% (a) and the arrangement of the atoms in the polyhedrons (b). In this view, hydrogen atoms are omitted for clarity.

Table 2
Selected bond lengths (Å) and angles (°) for $[Eu(ODA)\cdot(phen)\cdot 4H_2O]^+$ complex

Eu–O15	2.346(3)	Eu–O19	2.530(3)
Eu–O22	2.368(3)	Eu–N1	2.609(4)
Eu–N12	2.597(4)	Eu–OW1	2.512(4)
Eu–OW2	2.436(3)	Eu–OW3	2.468(3)
Eu–OW4	2.486(4)		
O15–Eu–O22	126.60(11)	O15–Eu–OW2	78.71(12)
O22–Eu–OW2	140.27(12)	O15–Eu–OW3	144.64(12)
O22–Eu–OW3	73.14(12)	OW2–Eu–OW3	70.92(13)
O15–Eu–OW4	81.81(14)	O22–Eu–OW4	76.53(14)
OW2–Eu–OW4	142.36(14)	OW3–Eu–OW4	133.53(14)
O15–Eu–OW1	83.05(13)	O22–Eu–OW1	80.36(12)
OW2–Eu1–OW1	72.48(13)	OW3–Eu1–OW1	71.04(13)
OW4–Eu–OW1	136.35(14)	O15–Eu–O19	62.77(10)
O22–Eu–O19	63.93(10)	OW2–Eu–O19	126.87(12)
OW3–Eu–O19	124.06(11)	OW4–Eu–O19	68.63(12)
OW1–Eu–O19	68.02(12)	O15–Eu–N12	135.09(11)
O22–Eu–N12	80.11(11)	OW2–Eu–N12	103.45(13)
OW3–Eu1–N12	71.23(12)	OW4–Eu1–N12	69.51(13)
OW1–Eu–N12	141.10(12)	O19–Eu–N12	129.59(11)
O15–Eu1–N1	75.91(11)	O22–Eu1–N1	138.67(12)
OW2–Eu–N1	70.97(12)	OW3–Eu–N1	109.50(12)
OW4–Eu–N1	73.20(13)	OW1–Eu–N1	140.60(12)
O19–Eu–N1	126.36(11)	N12–Eu–N1	63.32(11)

Table 3
Selected bond lengths (Å) and angles (°) for $[Tb(ODA)\cdot(phen)]^+$ complex

Tb–O15	2.324(3)	Tb–O19	2.519(3)
Tb–O22	2.349(4)	Tb–OW4	2.457(4)
Tb–OW1	2.484(4)	Tb–OW2	2.409(4)
Tb–OW3	2.448(4)	Tb–N1	2.580(4)
Tb–N12	2.572(4)		
O15–Tb–O19	63.24(12)	O15–Tb–O22	127.39(13)
O15–Tb–N1	75.39(14)	O15–Tb–N12	135.16(14)
O19–Tb–O22	64.23(12)	O19–Tb–N1	126.39(13)
O19–Tb–N12	129.42(13)	N1–Tb–N12	63.36(14)
O15–Tb–OW4	82.08(13)	O15–Tb–OW1	83.15(13)
O15–Tb–OW2	78.34(14)	O15–Tb–OW3	144.38(13)
O22–Tb–OW4	76.94(14)	O22–Tb–OW1	80.37(13)
O22–Tb–OW2	140.04(13)	O22–Tb–OW3	72.86(14)
O22–Tb–N1	138.90(14)	O22–Tb–N12	79.63(13)
OW4–Tb–O19	68.96(13)	OW4–Tb–OW1	136.65(13)
OW4–Tb–OW2	142.08(13)	OW4–Tb–OW3	133.50(13)
OW4–Tb–N1	73.10(14)	OW4–Tb–N12	69.28(13)
OW1–Tb–O19	67.98(13)	OW1–Tb–OW2	72.54(13)
OW1–Tb–OW3	71.05(13)	OW1–Tb–N1	140.32(13)
OW1–Tb–N12	140.93(13)	OW2–Tb–O19	126.92(13)
OW2–Tb–OW3	70.86(13)	OW2–Tb–N1	70.69(13)
OW2–Tb–N12	103.58(14)	OW3–Tb–O19	124.06(13)
OW3–Tb–N1	109.49(14)	OW3–Tb–N12	71.11(14)

2.526(5) Å). The angle formed by Eu and the two carboxylate oxygen atoms is 126.60(11)°. This angle equals the average value of 126.60(11)° of $[Er(ODA)\cdot(phen)\cdot 4H_2O]^+$.

Nine-coordinated Ln(III) complexes most frequently form tricapped trigonal prism (TCTP) or capped square antiprism (CSAP) polyhedrons. As shown in Fig. 1(b), the TCTP geometry can be accessed using the three rectangular (O15–Ow4–O22–Ow1, O15–Ow4–N12–Ow2, Ow1–O22–N12–Ow2) and two triangular (O15–Ow1–Ow2, Ow4–O22–N12) faces of the trigonal prism and the three atoms occupying the capping positions (O19, N1, Ow3). The dihedral angles (δ) between pairs of adjacent triangular faces, O19(O15Ow4)N1, N1(Ow2N12)Ow3 and Ow3(Ow1O22)O19), were calculated to be 32.21(19), 5.17(28) and 34.51(13)°, respectively. Significant deviation from the ideal TCTP geometry in the range of 25–30°, can be found in the 5.17(28)° of N1(Ow2N12)Ow3. This dihedral angle suggests that N1, Ow2, N12 and Ow3 are almost planar. The least-square equation of this plane is $8.002x - 10.476y + 2.702z = 3.888$. The N12 and Ow2 atoms are located 0.048 and 0.046 Å above the mean plane, respectively, while the N1 and Ow3 atoms are displaced in the opposite direction by 0.048 and 0.046 Å, respectively. The least-square equation of the plane formed by O15, Ow4, O22 and Ow1 is $8.246x - 9.755y + 2.968z = 1.667$. The Ow4 and Ow1 atoms are located 0.069 and 0.065 Å above the mean plane, respectively, while the O15 and O22 atoms are displaced in the opposite direction by 0.064 and 0.070 Å, respectively. In CSAP, the Eu(III) ion is located 0.967 Å below the upper plane (O15–Ow4–O22–Ow1) and 1.466 Å above the lower plane (N1–N12–Ow3–Ow2). The displacement of each atom from the mean plane shows that the Eu(III) complex forms a slightly distorted capped square polyhedron.

$[Tb(ODA)\cdot(phen)\cdot 4H_2O]^+$: The crystal structure of the Tb(III) complex is very similar to that of the Eu(III) complex. As listed in Table 3, the two Tb–carboxylate oxygen atom distances are 2.324(3) and 2.349(3) Å and the Tb–ether oxygen atom distance is 2.519(3) Å. The two Tb–N distances are 2.580(4) and 2.572(4) Å. These bond distances in $[Tb(ODA)\cdot(phen)\cdot 4H_2O]^+$ are slightly shorter than the respective distances in $[Eu(ODA)\cdot(phen)\cdot 4H_2O]^+$, while they are slightly longer than those in $[Er(ODA)\cdot(phen)\cdot 4H_2O]^+$ [4]. From this, it can be assumed that the bond distances of Ln(III)–N and Ln(III)–O decrease as the radius of the Ln(III) ion decreases.

Similarly to the case in $[Eu(ODA)\cdot(phen)\cdot 4H_2O]^+$, the dihedral δ angle of N1(N12Ow2)Ow3 in $[Tb(ODA)\cdot(phen)\cdot 4H_2O]^+$ is 4.96°. This small angle implies that the four atoms form a planar arrangement. The least-square equation of this plane is $7.993x + 10.389y + 2.712z = 2.829$. The N12 and Ow2 atoms are located 0.045 and 0.044 Å above their mean plane, respectively, while the N1 and Ow3 atoms are displaced in the opposite direction by 0.045 and 0.044 Å, respectively. In the CSAP geometry, the least-square equation of the upper plane formed by the O15, Ow4, O22 and Ow1 atoms is $8.222x + 9.728y + 2.941z = 5.3924$. The Ow4 and Ow1 atoms are located 0.065 and 0.062 Å above the mean plane, respectively, while the O15 and O22 atoms are displaced in the opposite direction by 0.061 and 0.066 Å, respectively. Accordingly, the polyhedron of the Tb(III) complex has a distorted CSAP geometry.

$[Tb(ODA)_3]^{3-}$: The complex crystallizes in the monoclinic space group *Cc*. Fig. 2(a) shows the crystal structure of $[Tb(ODA)_3]^{3-}$ unit and selected bond lengths and angles are

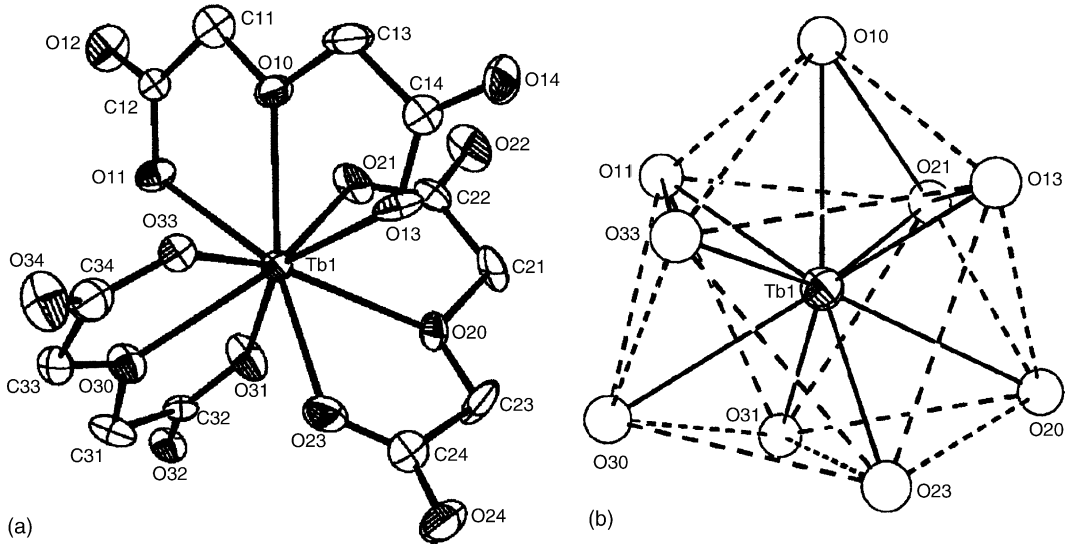

Fig. 2. View of the $[Tb(ODA)_3]^{3-}$ anion showing atom labeling and ellipsoids at 50% (a) and the arrangement of the atoms for the polyhedrons (b). In this view, hydrogen atoms are omitted for clarity.

given in Table 4. The average Tb–O distances are 2.484 and 2.371 Å for the three Tb–ether and six Tb–carboxylate oxygen bonds, respectively. Compared with the respective values for $[Tb(ODA)\cdot(phen)]^+$, the former is slightly shorter, while the latter is slightly longer. These values are very comparable with the respective values for $[Ln(ODA)_3]^{3-}$ crystals: 2.52 and 2.37 Å for Nd, 2.518 and 2.395 Å for Eu, 2.49 and 2.41 Å for Gd, and 2.46 and 2.31 Å for Yb, respectively [6–9]. The average bond angle of the six five-membered rings at the central Tb is 63.7°. The three angles subtended at the central Tb by the Tb–ether oxygen bonds are 115.57(14), 123.8(4) and 120.5(4)°. Their sum is 360.0°. The least-square equation of the plane containing the three ether oxygens and the Tb atoms is $2.689x - 0.018y + 16.439z = -4.089$. The three oxygen atoms are displaced by less than 0.008 Å below the mean plane, while the Tb atom is located 0.025 Å in the opposite direction. These four atoms form an almost planar geometry. Unlike to the cases of $[Eu(ODA)\cdot(phen)\cdot 4H_2O]^+$ and $[Tb(ODA)\cdot(phen)]^+$, the $[Tb(ODA)_3]^{3-}$ complex forms the TCTP geometry via the three rectangular (O11–O33–O13–O21, O21–O13–O23–O31, O31–O23–O33–O11) and the two triangular (O11–O21–O31, O13–O23–O33) faces of the trigonal prism and the three central oxygen atoms occupying the capping positions (O10, O20, O30), as shown in Fig. 2(b). The calculated δs between pairs of adjacent triangular faces, O10(O13O21)O20, O20(O23O31)O30 and O3(O33O11)O10, are 20.04(16), 27.06(54) and 28.90(50)°, respectively. These δ values show that the $[Tb(ODA)_3]^{3-}$ polyhedron is closer to the TCTP, than the CSAP. The least-square equations of the three rectangular faces are $-13.262x + 5.044y + 6.936z = 4.521$, $13.342x + 4.976y - 6.886z = 0.823$ and $0.107x + 9.803y - 0.099z = 0.823$, respectively. The dislocation of the composing atoms from their mean planes ranges from 0.174 to 0.207 Å. This implies that the $[Tb(ODA)_3]^{3-}$ polyhedron is distorted from the ideal TCTP with D_{3h} symmetry.

Table 4
Selected bond lengths (Å) and angles (°) for $[Tb(ODA)_3]^{3-}$ complex

Tb–O10	2.429(8)	Tb–O11	2.415(9)
Tb–O13	2.383(9)	Tb–O20	2.538(8)
Tb–O21	2.380(7)	Tb–O23	2.316(11)
Tb–O30	2.486(5)	Tb–O31	2.365(9)
Tb–O33	2.365(9)		
O10–Tb–O11	63.0(3)	O10–Tb–O13	63.2(3)
O10–Tb–O20	115.56(14)	O10–Tb–O21	70.4(3)
O10–Tb–O23	137.6(4)	O10–Tb–O30	120.6(4)
O10–Tb–O31	136.2(4)	O10–Tb–O33	75.1(3)
O11–Tb–O13	126.1(3)	O11–Tb–O20	136.5(3)
O11–Tb–O21	76.5(3)	O11–Tb–O23	148.36(14)
O11–Tb–O30	72.6(4)	O11–Tb–O31	80.3(4)
O11–Tb–O33	85.0(3)	O13–Tb–O20	73.1(3)
O13–Tb–O21	89.47(14)	O13–Tb–O23	78.1(3)
O13–Tb–O30	135.9(4)	O13–Tb–O31	147.9(3)
O13–Tb–O33	78.0(3)	O20–Tb–O21	64.0(3)
O20–Tb–O23	64.7(3)	O20–Tb–O30	123.8(4)
O20–Tb–O31	74.9(3)	O20–Tb–O33	138.3(3)
O21–Tb–O23	128.6(3)	O21–Tb–O30	134.4(4)
O21–Tb–O31	78.7(3)	O21–Tb–O33	145.3(3)
O23–Tb–O30	75.8(4)	O23–Tb–O31	86.2(4)
O23–Tb–O33	80.6(3)	O30–Tb–O31	63.8(4)
O30–Tb–O33	63.2(3)	O31–Tb–O33	127.08(13)

3.2. PL and excitation spectra

$[Eu(ODA)\cdot(phen)\cdot 4H_2O]^+$ and $[Eu(ODA)_3]^{3-}$: The PL spectra of $[Eu(ODA)\cdot(phen)\cdot 4H_2O]^+$ and $[Eu(ODA)_3]^{3-}$ crystals excited at the He–Cd 325 nm line were measured in the visible wavelength region at 10 K and room temperature. There was no significant difference between the two spectra, except that the intensity increased and the splitting sharpened at 10 K. As shown in Figs. 3(a) and 4(a), $[Eu(ODA)\cdot(phen)\cdot 4H_2O]^+$ and $[Eu(ODA)_3]^{3-}$ crystals pro-

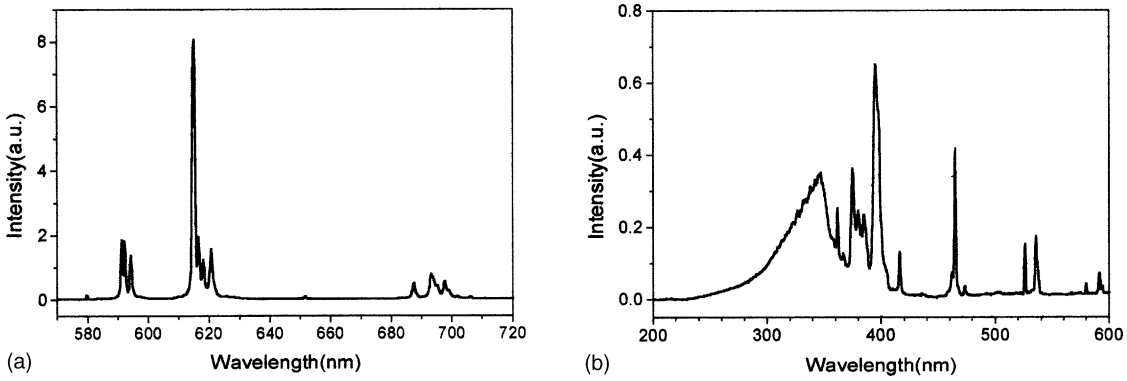

Fig. 3. PL (a) and excitation (b) spectra of $[Eu(ODA)\cdot(phen)\cdot 4H_2O]^+$ crystals at 10 K: (a) λ_{exc} = 325-nm laser and (b) λ_{ems} = 614 nm.

duced very typical band features in the wavelength region of 570–720 nm, arising mostly from the $^5D_0 \rightarrow {}^7F_J$ (J = 0, 1, 2, 3, 4) transitions of Eu(III). The $^5D_0 \rightarrow {}^7F_0$ transition is in principle forbidden, but may gain intensity through J mixing due to the crystal-field potential. For $[Eu(ODA)\cdot(phen)\cdot 4H_2O]^+$, however, this transition appeared with very weak intensity at 580 nm, while for $[Eu(ODA)_3]^{3-}$, this transition did not appear. Compared with the PL spectrum of the $[Eu(ODA)_3]^{3-}$ complex, the characteristic feature in the luminescence of $[Eu(ODA)\cdot(phen)\cdot 4H_2O]^+$ is found in the $^5D_0 \rightarrow {}^7F_1$ and $^7F_2$ transitions, appearing in the 585–600 nm and the 605–630 nm regions, respectively. Unlike other $^5D_0 \rightarrow {}^7F_J$ transitions, the $^5D_0 \rightarrow {}^7F_1$ transition is allowed by the magnetic dipole moment. Its intensity is almost independent of the environment and it has been observed with moderate intensity in most of Eu^{3+} complexes. For some Eu(III)/polycarboxylate complexes [14], the $^5D_0 \rightarrow {}^7F_2$ transition shows hypersensitivity, which is characterized by $\Delta J = 2$ when the site symmetry of the ion does not possess an inversion center. For the $[Eu(ODA)_3]^{3-}$ complex, the intensity of the $^5D_0 \rightarrow {}^7F_2$ transition increases with complexing with ODA. However, Its intensity is comparable with, but somewhat lesser than, that of the $^5D_0 \rightarrow {}^7F_1$ transition. The intensity of the $^5D_0 \rightarrow {}^7F_2$ transition of the $[Eu(ODA)\cdot(phen)\cdot 4H_2O]^+$ complex is strongly enhanced.

Excitation spectra of the strongest 614 nm emission from $[Eu(ODA)\cdot(phen)\cdot 4H_2O]^+$ and $[Eu(ODA)_3]^{3-}$ crystals were also measured at 10 K and room temperature. As shown in Figs. 3(b) and 4(b), the excitation spectrum of $[Eu(ODA)\cdot(phen)\cdot 4H_2O]^+$ is significantly different from that of the $[Eu(ODA)_3]^{3-}$ complex. A broad band, peaking at 345 nm, which was not found in the excitation spectrum of $[Eu(ODA)_3]^{3-}$ crystals, can be attributed to energy transfer from phen to Eu(III).

$[Tb(ODA)\cdot(phen)\cdot 4H_2O]^+$ and $[Tb(ODA)_3]^{3-}$: The PL spectra of $[Tb(ODA)\cdot(phen)\cdot 4H_2O]^+$ and $[Tb(ODA)_3]^{3-}$ crystals excited at the He–Cd 325 nm line were measured in the visible wavelength region at 10 K and room temperature. As shown in Figs. 5(a) and 6(a), the $[Tb(ODA)\cdot(phen)\cdot 4H_2O]^+$ and $[Tb(ODA)_3]^{3-}$ crystals produced very typical band features, originating from the transition from the $^5D_4$ state to the ^7F_J (J = 6–0). The band positions of the PL of $[Tb(ODA)\cdot(phen)\cdot 4H_2O]^+$ are almost identical to those of $[Tb(ODA)]^{3-}$, but the band splitting of the two complexes differs slightly. Significant differences between these two complexes can be found in the PL intensity and shape of the excitation spectrum. The PL intensity of $[Tb(ODA)\cdot(phen)\cdot 4H_2O]^+$ is markedly enhanced, compared with that of $[Tb(ODA)]^{3-}$. The medium-intensity 489-, 582- and 621-nm bands are attributed to the transitions from the $^5D_4$ state to the $^7F_6$, $^7F_4$ and $^7F_3$ states, respectively. These transitions show moderate sensitivity to the ligand environment. The most intense luminescence is observed in the $^5D_4 \rightarrow {}^7F_5$ transition peaking at 545 nm. This transition is the

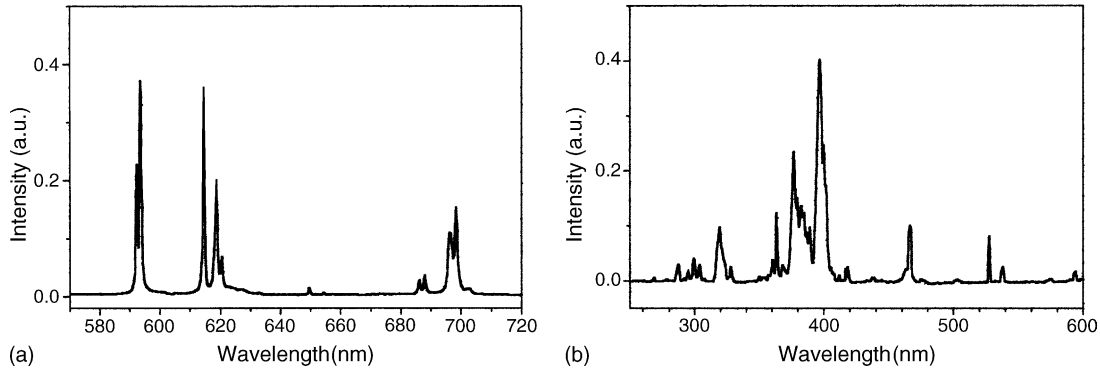

Fig. 4. PL (a) and excitation (b) spectra of $[Eu(ODA)_3]^{3-}$ crystals at 10 K: (a) λ_{exc} = 325-nm laser and (b) λ_{ems} = 614 nm.

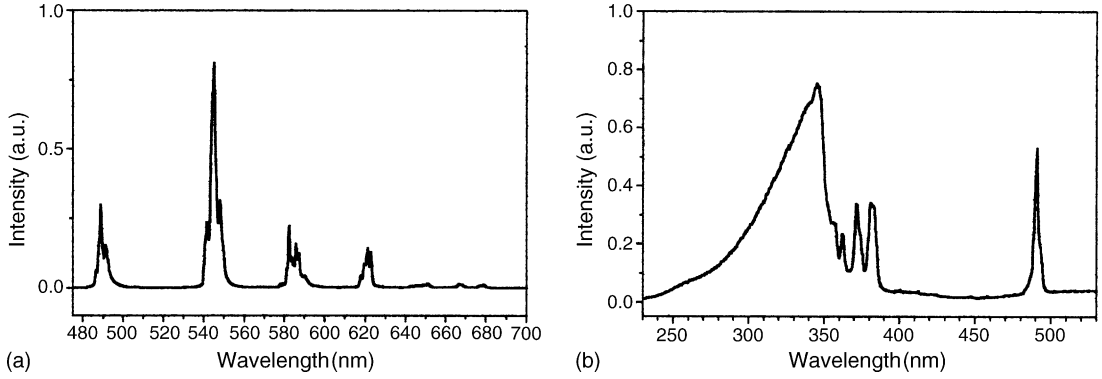

Fig. 5. PL (a) and excitation (b) spectra of $[Tb(ODA)\cdot(phen)\cdot 4H_2O]^+$ crystals at 10 K: (a) λ_{exc} = 325-nm laser and (b) λ_{ems} = 544 nm.

best probe transition. In addition, three $^5D_4 \rightarrow {}^7F_{2,1,0}$ transitions, peaking at 649, 668 and 679 nm, respectively, are very weak, as shown in the extended scale in Figs. 5(a) and 6(a).

Figs. 5(b) and 6(b) show the excitation spectra of the 544 nm emission band from $[Tb(ODA)\cdot(phen)\cdot 4H_2O]^+$ and $[Tb(ODA)_3]^{3-}$ crystals, respectively, measured at 10 K. For $[Tb(ODA)\cdot(phen)\cdot 4H_2O]^+$, a strong ligand-to-metal energy transfer band appeared at 344 nm, as seen in $[Eu(ODA)\cdot(phen)\cdot 4H_2O]^+$. This band is much stronger than the 488-nm band. For $[Tb(ODA)]^{3-}$, three characteristic bands appeared in the 300–520 nm wavelength region. The low-energy band peaking at 489 nm is attributed to the $^7F_6 \rightarrow {}^5D_4$ transition. For free Tb^{3+} ions, the multiplet ^5G_J and ^5L_J states are superimposed in the 25000–30000 cm^{-1} region. According to the Judd–Ofelt tensor matrix with the calculated energy levels and the observed oscillator strength for Tb^{3+} [15], the observed multiple 380 and 355 nm bands are attributed to the $^7F_6 \rightarrow {}^5D_3$, $^5G_6$ and $^5L_{10}$, and $^7F_6 \rightarrow {}^5G_5$ and $^5L_9$ transitions, respectively. For $[Tb(ODA)\cdot(phen)\cdot 4H_2O]^+$, the $^7F_6 \rightarrow {}^5D_4$ and the $^7F_6 \rightarrow {}^5D_3$, $^5G_6$ and $^5L_{10}$ transitions appeared at 489 and 385 nm, respectively. For $[Tb(ODA)\cdot(phen)\cdot 4H_2O]^+$, the intensity of the ligand-to-metal energy transfer band is very strong and broad enough to bury the 356 nm band, attribute to the $^7F_6 \rightarrow {}^5G_5$ and $^5L_9$ transitions.

3.3. Quantum yield and decay time

The absolute quantum yields of sensitized and non-sensitized luminescence of the complexes in crystalline state were precisely determined at room temperature. The results are listed in Table 5, For $[Eu(ODA)\cdot(phen)\cdot 4H_2O]^+$, the quantum yields of the non-sensitized luminescence (λ_{exc} = 397 nm) and the phen-sensitized luminescence (λ_{exc} = 345 nm) are only 2.0 and 6.6%, respectively. For $[Tb(ODA)\cdot(phen)\cdot 4H_2O]^+$, however, the quantum yields markedly increased to 24.0% for the non-sensitized luminescence (λ_{exc} = 379 nm) and to 75.7% for the phen-sensitized luminescence. For the homoleptic ODA complexes, the Tb(III) complexes produced more effective luminescence than the Eu(III) complex. As listed in Table 5, for $[Eu(ODA)_3]^{3-}$, Q is only 7.1%, while for $[Tb(ODA)_3]^{3-}$, Q (=21.0%) is three times as much as the case of $[Eu(ODA)_3]^{3-}$.

The probability for the energy transfer from the excited state of the ligand to rare earth ion has been taken into account along with the exchange-interaction theory described by Dexter [16]. The exchange interaction is active if the emission band of a sensitizer (S) overlaps the 4f–4f absorption band of the lanthanide ion. The probability of the energy transfer from a sensitizer to an acceptor, P_{ET} by the exchange

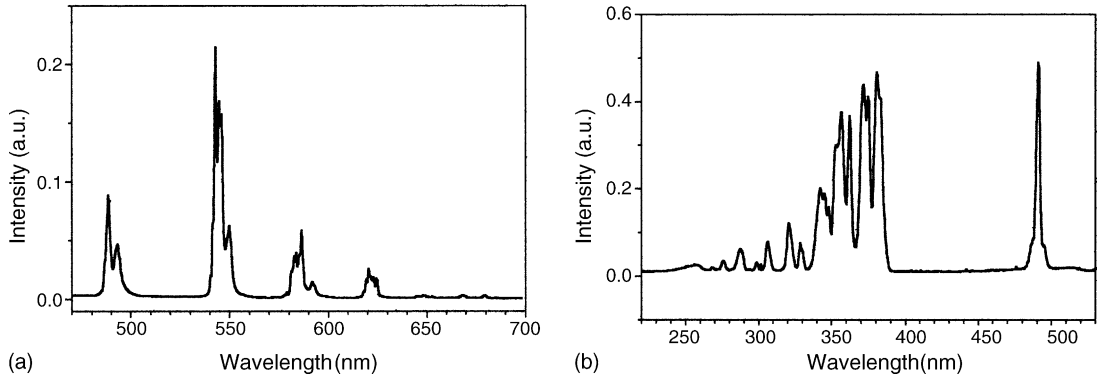

Fig. 6. PL (a) and excitation (b) spectra of $[Tb(ODA)_3]^{3-}$ crystals at 10 K: (a) λ_{exc} = 325-nm laser and (b) λ_{ems} = 544 nm.

Table 5
Absolute quantum yields (Q) and observed decay times (τ) of $[Eu(ODA)\cdot(phen)\cdot 4H_2O]^+$, $[Eu(ODA)_3]^{3-}$, $[Tb(ODA)\cdot(phen)\cdot 4H_2O]^+$ and $[Tb(ODA)_3]^{3-}$ complexes in crystalline state

Complex	Q (%)		τ (ms)	
	Sensitized	Non-sensitized	Sensitized	Non-sensitized
$[Eu(ODA)\cdot(phen)\cdot 4H_2O]^+$	6.6	2.0	0.27	0.28
$[Eu(ODA)_3]^{3-}$	–	7.1	–	1.1
$[Tb(ODA)\cdot(phen)\cdot 4H_2O]^+$	75.7	24.0	0.83	0.85
$[Tb(ODA)_3]^{3-}$	–	21.0	–	2.7

mechanism is expressed by

$$P_{ET} = \left(\frac{2\pi Z^2}{\hbar}\right) \int f_S(E) F_A(E) dE \quad (2)$$

where the integral is over the normalized emission spectrum of the sensitizer and the absorption band of the activator. For most of chromophores, the intermolecular energy transfer may take place from the triplet state of phen to the resonance level of the rare earth ions, so that the shape of the normalized emission spectrum of phen would be the phosphorescence component of phen. Tobita and co-workers [17] reported that the paramagnetic metal ion increases the intersystem crossing of the chelating ligand, resulting in a reduction of the fluorescence intensity and a subsequent increase in the phosphorescence intensity. Assuming that the paramagnetic effects of Eu(III) and Tb(III) are almost equal to that of Gd(III), the shape of the normalized emission spectrum of phen was taken from the PL spectrum of $[Gd(ODA)\cdot(phen)\cdot 4H_2O]^+$ complex. As shown in Fig. 7, the Gd(III) complex produces strong fluorescence band following weak phosphorescence band. These bands originated from phen, since the first excited $^6P_{7/2}$ state of Gd(III) is higher than the 325 nm excitation energy. The phosphorescence band (T) was resolved from the whole spectrum by using Gaussian band (see Fig. 7). The shape of the absorption curves of the Eu(III) and the Tb(III) were taken from the excitation spectra of the 610-nm emission from $[Eu(ODA)\cdot(phen)\cdot 4H_2O]^+$ and the 544-nm emission from $[Tb(ODA)\cdot(phen)\cdot 4H_2O]^+$,

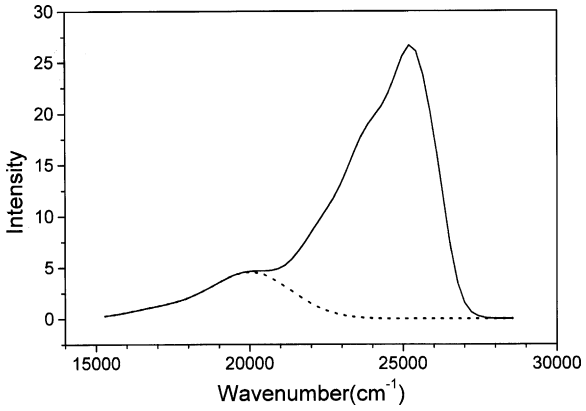

Fig. 7. PL spectrum of $[Gd(ODA)\cdot(phen)\cdot 4H_2O]^+$ crystals at room temperature (the dot line represents a phosphorescence component).

since it is difficult to obtain the absorption spectrum of the crystals. For $[Eu(ODA)\cdot(phen)\cdot 4H_2O]^+$, the overlap area between the T and the $^5D_2$ band was calculated to be five times more than that between the T and the $^5D_1$ band. For $[Tb(ODA)\cdot(phen)\cdot 4H_2O]^+$, only the $^5D_4$ band overlaps with the T band of phen.

In the Eq. (2), $Z^2 = K^2 \exp(-2R/L)$, where K is a constant with the dimension of energy, R is the separation between the sensitizer and the activator, and L is an effective average Bohr radius for the excited and unexcited states of the S and A. The quantity Z is associated with the overlap of electron clouds and cannot be derived from optical experiments. Moreover, it will depend strongly on the tails of the wave functions so that it is impossible to make any calculation of Z. For the case with an energy-overlap integral of $1/3\,eV^{-1}$, $R = 4$ Å and $L = 0.9$ Å, Dexter estimated P_{ET} to be 10^{10}–$10^{11}\,s^{-1}$. Assuming that L is half of the Ln–N distance, the vale of Z^2 for the Eu(III) and Tb(III) complexes is decreased by 1/2 times as much as the case estimated by Dexter [16]. With this approximation, we calculated the energy transfer probabilities of the complexes: for $[Eu(ODA)\cdot(phen)\cdot 4H_2O]^+$, P_{ET} $(T \rightarrow {}^5D_2) \cong 6 \times 10^{12}\,s^{-1}$ and P_{ET} $(T \rightarrow {}^5D_1) \cong 1.3 \times 10^{12}\,s^{-1}$, and for $[Tb(ODA)\cdot(phen)\cdot 4H_2O]^+$, P_{ET} $(T \rightarrow {}^5D_4) \cong 3 \times 10^{13}\,s^{-1}$.

In addition, the energy transfer from the singlet state of organic ligand to the lanthanide ion can be argued [18], since no emission from the phen moiety is observed, in contrast to the case of $[Gd(ODA)\cdot(phen)\cdot 4H_2O]^+$, for the mixed-ligand complex. For $[Eu(ODA)\cdot(phen)\cdot 4H_2O]^+$, the $^5L_6$ state at 25400 cm^{-1} lies near the excited singlet states of phen observed in the 21000–2700 cm^{-1} region. For $[Tb(ODA)\cdot(phen)\cdot 4H_2O]^+$, however, the second $^5G_{6,5}$ excited states of Tb(III) lie higher than the excited singlet states of phen, as shown in Fig. 5. Accordingly, the energy transfer from the singlet states of phen to the $^5D_4$ state of the Tb(III) ion can be negligible. It can lead us to assume that the energy transfer from the triplet states of phen to the lanthanide ions may predominate over any radiative and non-radiative processes occurring between the excited states and the ground state of the phen moiety. It could completely quench both fluorescence and phosphorescence from the phen moiety in the complex.

The luminescence decay curves of the complexes in crystalline state were measured at room temperature. Fig. 8 shows typical decay-curves fitted with single exponential decay time

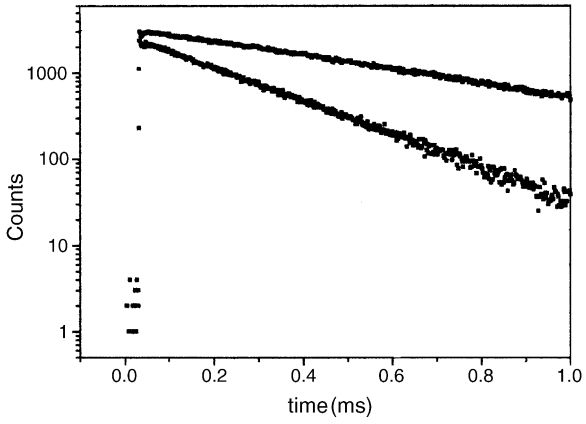

Fig. 8. Typical decay-time data for the 612 nm emission from Eu(ODA)·(phen)·4H$_2$O]$^+$ in crystalline (upper) and solution (lower) states.

in the microsecond range. For the complexes with ODA and phen, two times were determined: one is for the sensitized emission via the energy transfer from phen to the metal ion and the other is for the non-sensitized emission via the direct excitation of the metal ion. As listed in Table 5, these do not differ significantly. This could occur because the energy transfer rate from phen to the metal (ranged from 10^{12} to 10^{13} s^{-1}) is much faster than the luminescence rate (ranged from 10^3 to 10^4). As listed in Table 5, the lifetimes of the mixed-ligand complexes are three times shorter than those of the homoleptic ones for both the Eu(III) and Tb(III) complexes. It suggests that a deactivation channel may be present via the coordinated water molecules in the mixed-ligand complex. In other words, the OH vibration of water molecule may cause to decrease the quantum yield. In the case of the lifetime in absence of water molecule, the lifetime, τ, can be given as [2]

$$\tau = \left(k^\circ + \sum_i k_i^{nr}\right)^{-1} = \frac{1}{k} \quad (3)$$

where k° is the true rate-constant, k_i^{nr} is the relaxation rate-constant occurring in an i excited state, and k is the overall rate-constant. In presence of dynamic quenching due to water molecule coordinated to the metal ion, the lifetime can be rewritten as

$$\tau^q = \left(k^\circ + \sum_i k_i^{nr} + k_q\right)^{-1} \quad (4)$$

where k_q is the rate constant for the dynamic quenching responsible for the vibrational deactivation from the excited states of the lanthanide ion to water molecule. Taking τ from the lifetime of the homoleptic complex, $k_q = 2.7 \times 10^3$ s^{-1} for [Eu(ODA)·(phen)·4H$_2$O]$^+$ and $k_q = 8.1 \times 10^2$ s^{-1} for [Tb(ODA)·(phen)·4H$_2$O]$^+$. These results indicate that the deactivation due to water molecule for [Eu(ODA)·(phen)·4H$_2$O]$^+$ is three times more effective than that for [Tb(ODA)·(phen)·4H$_2$O]$^+$.

4. Conclusion

The crystal structures and luminescence properties of europium(III) and terbium(III) complexes with mixed ODA and phen ligands have been revealed. The X-ray structure confirms that the complexes form a slightly distorted CSAP polyhedron. The complexes upon the 325-nm excitation produce the characteristic line splitting which are responsible for the $^5D_0 \rightarrow {}^7F_J$ transitions for Eu(III) and the $^5D_4 \rightarrow {}^7F_J$ transitions for Tb(III). Among the complexes studied in this work, the terbium complex with ODA and phen is very luminescent materials. The luminescence intensity of the complex is strongly enhanced by the energy transfer from the phen to the Tb(III) ion. The quantum yield of the sensitized luminescence of the Tb(III) complex is very high (ca. 75%).

Acknowledgment

This work is funded by the Korean Science and Engineering Foundation (KOSEF R01-2001-00055).

Supporting information available: an X-ray crystallographic files (CIF) for [Eu(ODA)·(phen)·4H$_2$O]Cl·5H$_2$O, [Tb(ODA)·(phen)·4H2O]Cl·5H$_2$O and Na$_3$[Tb(ODA)$_3$]·8H$_2$O. These materials are available free of charge via jgkang@cnu.ac.kr.

References

[1] F.S. Richardson, Chem. Rev. 82 (1982) 541.
[2] J.-C.G. Bünzli, in: J.-C.G. Bünzli, G.R. Choppin (Eds.), Lanthanide Probes in Life, Chemical and Earth Sciences, Elsevier, Amsterdam, Oxford, New York, Tokyo, 1989 (Chapter 7).
[3] (a) M.D. McGehee, T.B. Bergstedt, C. Zhang, A.P. Saab, M.B. O'Regan, G.C. Bazan, V.I. Srdanov, A.J. Heeger, Adv. Mater. 11 (1999) 1349;
(b) W. Hu, M. Matsumura, M. Wang, L. Jin, Appl. Phys. Lett. 77 (2000) 26;
(c) Y. Zheng, J. Lin, Y. Liang, Q. Lin, J. Yu, Q. Meng, Y. Zhou, S. Wang, H. Wang, H. Zhang, J. Mater. Chem. 11 (2001) 2615;
(d) Y. Zheng, L. Fu, Y. Zhou, J. Yu, Y. Yu, S. Wang, H. Zhang, J. Mater. Chem. 12 (2002) 919.
[4] (a) J.-M. Lehn, Angew Chem. Int. Ed. Engl. 29 (1990) 1304;
(b) G.F. de Sá, O.L. Malta, C. Donegá, A.M. de Mello, R.L. Simas, P.A. Longo, E.F. Sata-Cruz, da Silva Jr., Coord. Chem. Rev. 196 (2000) 165.
[5] J.-G. Kang, T.-J. Kim, K.S. Park, S.K. Kang, Bull. Korean Chem. Soc. 25 (2004) 373.
[6] (a) J. Albertsson, Acta Chem. Scand. 22 (1968) 1562;
(b) J. Albertsson, Acta Chem. Scand. 24 (1970) 1213;
(c) J. Albertsson, Acta Chem. Scand. 24 (1970) 3527.
[7] F.R. Fronczek, A.K. Banerjee, S.F. Watkins, R.W. Schwartz, Inorg. Chem. 20 (1981) 2745.
[8] M. Albin, R.R. Whittle, W.DeW. Horrocks Jr., Inorg. Chem. 24 (1985) 4591.
[9] K.A. Schoene, J.R. Quagliano, F.S. Richardson, Inorg. Chem. 30 (1991) 3803.
[10] SHELXTL, 5.030 ed., Brucker Analytical X-ray Instruments Inc., Madison, WI, 1998.
[11] G.M. Sheldrick, SHELEX97, University of Göttingen, 1997.

[12] K.-B. Kim, Y.-I. Kim, H.-G. Chun, T.-Y. Cho, J.-S. Jung, J.-G. Kang, Chem. Mater. 14 (2002) 5045.
[13] J.C. de Mello, H.F. Wittmann, R.H. Friend, Adv. Mater. 9 (1997) 230.
[14] (a) J.-G. Kang, S.-K. Yoon, Y. Sohn, J.-G. Kim, Y.-D. Kim, I.-H. Suh, J. Chem. Soc. Dalton Trans. (1999) 1467;
(b) R. Baggio, M.T. Garland, M. Perec, D. Vega, Inorg. Chem. 35 (1996) 2399.
[15] W.T. Carnall, P.R. Fields, K. Rajnak, J. Chem. Phys. 49 (1968) 4412.
[16] D.L. Dexter, J. Chem. Phys. 21 (1953) 836.
[17] (a) S. Tobita, M. Arakawa, I. Tanaka, J. Phys. Chem. 88 (1984) 2697;
(b) S. Tobita, M. Arakawa, I. Tanaka, J. Phys. Chem. 89 (1985) 5649.
[18] (a) O.L. Malta, H.F. Brito, J.F.S. Menezes, F.R. Gonçalves e Silva, S. Alves Jr., F.S. Farias Jr., A.V.M. de Andrade, J. Lumin. 75 (1997) 255;
(b) R. Longo, F.R. Gonçalves e Silva, O.L. Malta, Chem. Phys. Lett. 328 (2000) 67.